



A TEMPOL and rapamycin loaded nanofiber-covered stent favors endothelialization and mitigates neointimal hyperplasia and local inflammation

Rui Wang^{a,c,1}, Jian Lu^{b,1}, Jiasheng Yin^{a,c,1}, Han Chen^{a,c}, Hongmei Liu^b, Fei Xu^{a,c}, Tongtong Zang^{a,c}, Rende Xu^{a,c,d}, Chenguang Li^{a,c,d}, Yizhe Wu^{a,c,d}, Qilin Wu^b, Xiang Fei^{b,***}, Meifang Zhu^{b,***}, Li Shen^{a,c,d,**}, Junbo Ge^{a,c,d,*}

^a Department of Cardiology, Zhongshan Hospital, Fudan University, Shanghai Institute of Cardiovascular Diseases, National Clinical Research Center for Interventional Medicine, Shanghai, China

^b State Key Laboratory for Modification of Chemical Fibers and Polymer Materials, College of Materials Science and Engineering, International Joint Laboratory for Advanced Fiber and Low-dimension Materials, Donghua University, Shanghai, 201620, China

^c Research Unit of Cardiovascular Techniques and Devices, Chinese Academy of Medical Sciences, Shanghai, China

^d Shanghai Engineering Research Center of Interventional Medicine, Shanghai, China

ARTICLE INFO

Keywords:

Electrospun nanofiber membrane
In-stent restenosis
Re-endothelialization
Reactive oxygen species

ABSTRACT

An increased level of reactive oxygen species (ROS) plays a major role in endothelial dysfunction and vascular smooth muscle cell (VSMC) proliferation during in-stent thrombosis and restenosis after coronary artery stenting. Herein, we report an electrospun core-shell nanofiber coloaded with 4-hydroxy-2,2,6,6-tetramethylpiperidine 1-oxyl (TEMPOL) and rapamycin (RAPA) that correspondingly serves as an ROS scavenger and VSMC inhibitor. This system has the potential to improve the biocompatibility of current drug-eluting stent (DES) coatings with the long-term and continuous release of TEMPOL and rapamycin. Moreover, the RAPA/TEMPOL-loaded membrane selectively inhibited the proliferation of VSMCs while sparing endothelial cells (ECs). This membrane demonstrated superior ROS-scavenging, anti-inflammatory and antithrombotic effects in ECs. In addition, the membrane could maintain the contractile phenotype and mitigate platelet-derived growth factor BB (PDGF-BB)-induced proliferation of VSMCs. *In vivo* results further revealed that the RAPA/TEMPOL-loaded covered stents promoted rapid restoration of vascular endothelium compared with DES and persistently impeded inflammation and neointimal hyperplasia in porcine models.

1. Introduction

Cardiovascular diseases (CVDs) remain the leading cause of global mortality and are a major contributor to disability [1], resulting in approximately 18 million CVD deaths and 17 million disability-adjusted life years annually [2]. To date, percutaneous coronary intervention (PCI) has been widely applied to treat ischemic heart disease as a

nonsurgical approach [3]. However, PCI-related complications, such as restenosis and stent thrombosis, still occur at a relatively high rate and limit the procedure's long-term success [4,5].

Neointima hyperplasia (NIH), which leads to in-stent restenosis (ISR), is a complex and time-dependent phenomenon that occurs in response to deep vascular injury, metal struts and stent polymers after stent implantation. This condition is characterized by VSMC migration

Peer review under responsibility of KeAi Communications Co., Ltd.

* Corresponding author. Department of Cardiology, Zhongshan Hospital, Fudan University, Shanghai Institute of Cardiovascular Diseases, National Clinical Research Center for Interventional Medicine, Shanghai, China.

** Corresponding author. Department of Cardiology, Zhongshan Hospital, Fudan University, Shanghai Institute of Cardiovascular Diseases, National Clinical Research Center for Interventional Medicine, Shanghai, China.

*** Corresponding author.

**** Corresponding author.

E-mail addresses: xiangfei@dhu.edu.cn (X. Fei), zmf@dhu.edu.cn (M. Zhu), shen.li1@zs-hospital.sh.cn (L. Shen), ge.junbo2@zs-hospital.sh.cn (J. Ge).

¹ These authors have contributed equally to this work.

<https://doi.org/10.1016/j.bioactmat.2022.04.033>

Received 26 February 2022; Received in revised form 12 April 2022; Accepted 28 April 2022

2452-199X/© 2022 The Authors. Publishing services by Elsevier B.V. on behalf of KeAi Communications Co. Ltd. This is an open access article under the CC BY-NC-ND license (<http://creativecommons.org/licenses/by-nc-nd/4.0/>).

and proliferation, induced mainly by inflammation and ROS production [6,7]. Drug-eluting stents (DESs), embedded in an antiproliferative drug-eluting polymer, were developed to avoid such secondary complications [8,9]. Antiproliferative drugs, such as rapamycin (RAPA) and rapamycin analogs (everolimus, biolimus A9, or zotarolimus), can effectively inhibit early in-stent restenosis by inhibiting the proliferation of VSMCs. However, despite the routine use of dual antiplatelet therapy, stent-associated thrombosis may occur after DES implantation. Delayed re-endothelialization is believed to be the primary cause of late thrombotic events in a well-deployed DESs [10]. In addition to antiproliferative drug-induced delayed re-endothelialization, vascular inflammation and ROS production have also been identified as contributors to in-stent thrombosis [6].

In our previous work, an antioxidant and anti-inflammatory molecule, 4-hydroxy-2,2,6,6-tetramethylpiperidine 1-oxyl (TEMPOL), was loaded in an electrospun membrane to alleviate the harmful effects of ROS, reducing VSMC migration and protecting ECs from inflammatory injury [11]. However, TEMPOL exhibited a weakened inhibitory effect on VSMC proliferation [12], and this issue is assumed to be effectively solved by introducing rapamycin analogs. Conversely, the ROS scavenging roles of TEMPOL may be complementary to rapamycin analogs to preserve endothelial functions while inhibiting VSMCs. Therefore, the combination of TEMPOL and rapamycin is promising when used as a stent coating for DES.

Electrospinning technology has been demonstrated as a promising method to incorporate bioactive substances into core-shell bioresorbable electrospun nanofibers for stent coating, artificial vessel grafting and other biomedical applications [13–15]. Electrospinning is an ideal approach for fabricating bioresorbable, nanofibrous stent coatings with desirable features, such as mimicking the natural extracellular matrix morphology and providing a higher specific surface area and a suitable microenvironment for cell attachment and proliferation [16].

Therefore, in this study, a first attempt at a combination of RAPA and TEMPOL was used to prevent VSMC proliferation without inhibition of ECs by employing RAPA/TEMPOL-loaded poly(lactic acid) (PLA)/poly(vinyl alcohol) (PVA) electrospun nanofibrous membranes as the drug release system. The manufacturing process, morphology, and drug release of the membrane were studied. Human umbilical vein endothelial cells (HUVECs) and rat thoracic aorta smooth muscle cells (RASMCs) were chosen for *in vitro* cell experiments. The effects of RAPA/TEMPOL-loaded membranes on cell viability, endothelial barrier integrity and cell inflammation conditions were evaluated in HUVECs. RASMCs were utilized to investigate the antiproliferative and proapoptotic effects as well as the anti-phenotype switching effect of the RAPA/TEMPOL-loaded membranes. Furthermore, the *in vivo* anti-restenosis and re-endothelialization performance of the RAPA/TEMPOL-loaded membranes as stent coatings was evaluated in a porcine coronary artery stenting model.

2. Materials and methods

2.1. Preparation and characterization of RAPA/TEMPOL-loaded PLA electrospun membranes

The shell solution was prepared by dissolving PLA (Mw = 300 kDa,

Jinan Daigang Biomaterial Co., China) in Hexafluoroisopropanol (HFIP, Shanghai Darui Finechem Co., China) with a concentration of 10% (w/v) and stirring at room temperature for 12 h. Then, RAPA (Aladdin Reagent Co., China) was added and dissolved for 1 h. A series of core solutions were prepared by dissolving TEMPOL (Aladdin Reagent Co., China) in 7.5% (w/v) PVA (Anhui Wanwei Group Co., Ltd., China) aqueous solution (which was stirred at 60 °C for 1 h and then at 90 °C for another 12 h) followed by room temperature stirring for over 0.5 h. Their concentrations are listed in Table 1. A coaxial electrospinning setup was used to prepare the RAPA/TEMPOL-loaded PLA electrospun membranes, as shown in Fig. 1a. The solutions for coaxial electrospinning were as follows: TEMPOL/PVA aqueous solution and RAPA/PLA in HFIP solutions. For the subsequent coaxial electrospinning, the internal diameters of the coaxial spinneret were 0.34 mm and 1.06 mm. The shell and core solution were pushed by a syringe pump at speeds of 1 mL/h and 0.1 mL/h, respectively, applied with a high voltage of 15 kV, and the collection distance was fixed to 15 cm. As a control, the same shell solutions without RAPA and core solutions without TEMPOL were also applied to prepare the nanofibrous membranes. In this work, all the electrospun membranes were collected for 1 h on a rotating drum (with a diameter of 7.8 cm) followed by vacuum drying at 40 °C for more than 12 h to remove residual solvent for further usage. The samples prepared with the same 1% (w/v) RAPA in the shell solution and different TEMPOL concentrations in core solutions of 0% (w/v), 0.4% (w/v), 2% (w/v), and 10% (w/v) were named P-R1-T0, P-R1-T0.4, P-R1-T2 and P-R1-T10, respectively; the optimal one among the above, P-R1-T2, and its control samples without RAPA and without both RAPA and TEMPOL, named P-R0-T2 and P-R0-T0, respectively, were used (Table S1).

Scanning electron microscopy (SEM) images were obtained with a Hitachi SU8010 system (Japan). Transmission electron microscopy (TEM) images were obtained with a JEM-2100 system (Japan).

2.2. *In vitro* release behaviors of RAPA/TEMPOL-loaded PLA nanofibers

To evaluate the release behavior of TEMPOL and RAPA from the nanofibers, we immersed membranes in 4 mL of phosphate-buffered saline (PBS, pH = 7.4) at 37 °C for release for certain time intervals; 1 mL of the above solution was then taken and used for the following high-performance liquid chromatography (HPLC, LC 2050, China) analysis. The amounts of RAPA and TEMPOL were tested with a mobile phase consisting of acetonitrile:water = 75/25 (v/v). An equal volume of fresh PBS was added to the stock solution for subsequent release incubations. The release percentage was calculated with the equation as follows:

$$M_t = M_1 + M_2 + \dots + M_x$$

where M_t is the cumulative amount of drug released from the electrospun membrane at predetermined time t , and M_x ($x = 1, 2, 3 \dots$) is the amount of drug in 1.0 mL PBS at predetermined time.

2.3. *In vitro* performance

2.3.1. Cell culture

Each sample was cut into approximately 1.5 × 1.5 cm pieces to match the size of 12-well culture plates (Costar, USA) with a density of 0.6316–0.7895 mg/cm². All the samples were stored at 4 °C and

Table 1
Primers used in qRT-PCR.

Gene	Forward primer sequence (5'–3')	Reverse primer sequence (5'–3')
VCAM-1	GATTCTGTGCCACAGTAAGGC	TGGTCACAGAGCCACCTTCTTG
TF	CAGAGTTCACACCTTACCTGGAG	GTTGTTCTCTTGACTAAAGTCCG
E-selectin	GGACACCACAAAATCCCAGTCTG	TGCAGGAGAACTCACAACCTGG
PAI-1	GGACACCACAAAATCCCAGTCTG	TGCAGGAGAACTCACAACCTGG
GAPDH	GTCTCCTGACTTCAACAGCG	ACCACCTGTTGCTGTAGCCAA

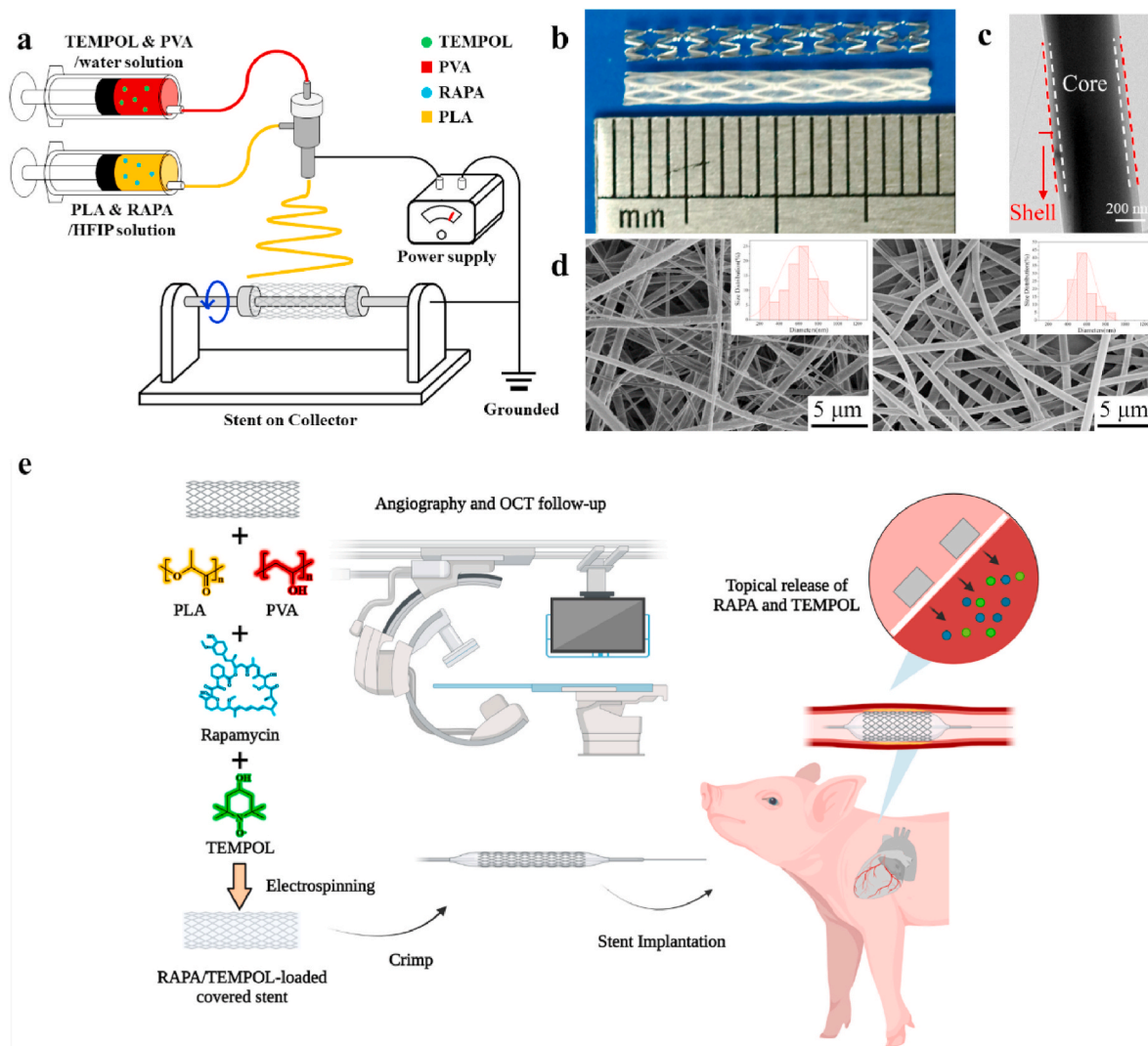


Fig. 1. Development of a RAPA/TEMPOL-loaded nanofibrous coating for the vascular stent. (a) Schematic illustration for the preparation of RAPA/TEMPOL-loaded PLA electrospun fibrous coating; (b) A digital photo of the stent without and with the nanofiber coating; (c) A representative TEM image of the P-R1-T2 nanofiber; (d) SEM images and corresponding diameter quantitative analysis of the nanofibers (left) without and (right) with RAPA/TEMPOL-loaded; e Schematic illustration for stent deployment in porcine coronary arteries with coating topically releasing TEMPOL and RAPA to the vessel wall.

sterilized under ultraviolet light for 2 h. Stainless steel rings ($\Phi = 20$ mm, $\varphi = 12$ mm, $\delta = 2.0$ mm) were used to prevent the membranes from floating. Cells were seeded on membranes in 12-well plates at a certain concentration.

Primary HUVECs were obtained from ScienCell Research Laboratories (USA). Cells were provided at passage 1 and cultured in ECM (ScienCell Research Laboratories, USA) with 5% FBS, 1% endothelial cell growth supplement (ECGS) and 1% penicillin-streptomycin. RASMCs were obtained from the National Collection of Authenticated Cell Cultures (China). These cells were maintained in DMEM (Gibco, USA) with 10% FBS (Gibco, USA). Cells were cultured at 37 °C/5% CO₂, and cells at the 3rd to 6th passages were used in the later experiments.

2.3.2. Cell proliferation assay

For the cell viability study, 1 mL of 2×10^5 HUVECs was seeded on electrospun nanofibrous membranes in 12-well culture plates and quantified at 24 h, 72 h and 120 h by CCK-8 assays (Dojindo Laboratories, Japan).

For evaluation of the inhibition of membrane VSMC proliferation, RASMCs were seeded onto membranes at a density of 1×10^5 cells in 1 mL/well and allowed to attach for 6–8 h. For the time course

experiment, cells were cultured for 1 day, 3 days and 5 days. Cell proliferation was evaluated at each time point by CCK-8 assays. The optical density was read by a microplate reader at a wavelength of 486 nm. For EdU analysis, cells after 60 h of platelet-derived growth factor BB (PDGF-BB) treatment were incubated with EdU (RiboBio, China) for another 12 h. The nuclei were counterstained with 4,6-diamidino-2-phenylindole (DAPI, Weiao Biotech, China), and the images were captured by fluorescence microscopy (Leica, Germany).

2.3.3. Endothelial permeability assay

HUVECs were seeded into the upper compartment of a Transwell chamber (Corning, USA) with a pore size of 0.4 μ m. HUVECs were cultured for 2 days before attaching electrospun nanofibrous membranes to the bottom of the upper compartment and incubated for an additional 3 days. Fluorescein isothiocyanate (FITC)-coupled dextran with a molecular weight of 70 kDa (Sigma, USA) was added to the upper compartment prior to the indicated time points. The fluorescence of FITC-dextran (Ex485 nm/Em535 nm) in the lower compartment was measured by a microplate reader equipped for fluorescence measurement (Multishan Go, Biotek, USA). Endothelial permeability was expressed as the OD value of the medium in the lower compartment.

2.3.4. Cell apoptosis assay

Cell apoptosis status was evaluated by terminal deoxynucleotidyl transferase (TdT)-mediated dUTP nick end labeling (TUNEL, Beyotime Biotech, China) staining according to the manufacturer's protocol. Phalloidin (AAT Bioquest, USA) and DAPI were stained simultaneously with TUNEL to identify the cell configuration and cell nuclei.

2.3.5. ROS-scavenging capability

ROS production was evaluated using 2,7-dichlorodihydrofluorescein diacetate (DCFH-DA, Sigma, USA) staining. HUVECs and RASMCs were seeded on electrospun membranes for 3 days in complete medium before stimulation with 0.8 mM H₂O₂ (Sigma, USA) for 16 h and 20 ng/mL PDGF-BB for 24 h, respectively. Cells were digested with 0.05% trypsin (Gibco, USA) and collected in 1.5 mL microcentrifuge tubes (Eppendorf, Germany). Complete medium with DCFH-DA (10 mM, Sigma, USA) was used to resuspend collected cells, which were incubated for 1 h at 37 °C. DCFH-DA was discarded, and the cells were washed twice with cold PBS. Then, the cells were resuspended in 1 mL of complete medium per sample. DCFH-DA-positive cells were identified and recorded by flow cytometry (Becton, Dickinson and Company, USA).

2.3.6. Anti-inflammatory capacity of HUVECs

HUVECs were cultured on the membranes for 3 days to reach over 80% confluence before the cells were stimulated with 10 ng/mL TNF α (PeproTech, USA) for 2 h. Thereafter, the cells were collected, and total RNA was extracted for further qRT-PCR.

Total RNA was extracted using an adsorption column-based extraction kit (Tiangen Biotech, China) according to the manufacturer's instructions. For gene expression analysis, isolated RNA was reverse transcribed using PrimeScript RT Master Mix (TaKaRa, Japan). qRT-PCR was performed in triplicate using TB Green Premix Ex Taq II (TaKaRa, Japan) with a CFX96 real-time PCR system and CFX Manager Software (Bio-Rad Laboratories, Germany). Samples were normalized to the expression of GAPDH for gene expression targets. Target relative amounts were calculated using the 2^{- $\Delta\Delta$ CT} method. The qRT-PCR primers were as follows:

2.3.7. Immunoblot analysis of HASMCs

Protein extracted from cells was denatured at 95 °C, reduced with sample buffer (0.1 mol/L Tris, pH 6.8, 40% glycerol, 2% SDS, 2% beta-mercaptoethanol and 0.02% bromophenol blue) and separated by SDS-PAGE. Then, the proteins were blotted onto a nitrocellulose membrane, which was blocked in 5% BSA and incubated with primary antibodies against calponin (CNN1, Proteintech, 24844-1-AP, USA), transgelin (SM22a, Proteintech, 10493-1-AP, USA), osteopontin (OPN, Proteintech, 22952-1-AP, USA), proliferating cell nuclear antigen (PCNA, Cell Signaling Technology, 13110, USA) and β -actin (Cell Signaling Technology, 4970, USA) overnight. Subsequently, the membranes were treated with HRP-conjugated light chain-specific detection antibody (1:5000, Weiao Biotech, China) for 1 h. The membranes were developed using chemiluminescence (Millipore, WBLUF0500) on an Xograph processor (Bio-Rad Laboratories, GelDoc Go, Germany).

2.4. In vivo performance

2.4.1. Stent preparation

Bare metal stents (BMS, 3.0 \times 17 mm, 316L stainless steel, JW medical system, China) were laser cut from the stent tube (Φ = 1.8 mm), and subjected to stent coating. For the stent coating, P-R1-T2 was prepared according to the method above and collected with a rotation of BMS for 138 s. Coated stents were cramped onto balloon catheters using tweezers and sterilized by beta radiation prior to *in vivo* use.

2.4.2. Porcine model of stent implantation

All porcine animal procedures were approved by the local ethical committee for animal experiments, Zhongshan Hospital, Fudan

University, Shanghai, China. Eight male and female mini pigs (3–6 months old, 35–45 kg) underwent percutaneous coronary intervention by transfemoral access (n = 5/stent group). All pigs received a loading dose of aspirin and clopidogrel orally before the procedure and maintained the dual antiplatelet therapy until sacrifice (by propofol overdose followed by perfusion with a saturated KCl solution, under general anesthesia). Three coronary arteries [left anterior descending (LAD), left circumflex (LCX), and right coronary arteries (RCA)] of each animal were stented. Either a BMS or a drug-eluting stent (DES, EXCEL[®], 3.0 \times 17 mm, JW Medical System, China) or a RAPA/TEMPOL-loaded covered stent (RTCS, 3.0 \times 17 mm) was randomly stented in the porcine coronary artery. Angiography and optical coherence tomography (OCT, St. Jude Medical, USA) were performed 2 weeks, 1 month and 3 months after stent implantation, followed by harvesting of coronary arteries.

2.4.3. OCT image analysis in pigs

OCT imaging was performed at stent implantation and at follow-up using the Iliumien Optis imaging system (St. Jude Medical, USA) according to previously published methods [17]. Briefly, the OCT catheter (Dragonfly Optis, St. Jude Medical, USA) was positioned at least 5 mm distal to the stent, and automated pullback was triggered by hand injection of 6–8 mL contrast. The analysis of contiguous cross-sections was performed at every frame within the segment to assess the minimal lumen area, stent area, stent strut coverage and neointimal volume consistent with previously validated methodologies (Supplemental file). The data were analyzed using the OCT image analysis system, QIVUS3.0 Version with OCT Module (Medis Medical Imaging, Netherlands).

2.4.4. ROS-scavenging capability in vivo

Stent struts were carefully removed under a stereomicroscope shortly after artery explantation. Strut-free vessels were embedded in optimal cutting temperature compound (Sakura Finetek, USA) and stored at –80 °C before final processing (within 72 h). The vessel sections were equilibrated at room temperature for 0.5 h before incubation with 10 μ M DCFH-DA for 30 min at 37 °C. DCFH-DA was removed, and sections were rinsed with PBS 3 times before imaging. Images were captured by digital fluorescence slide scanner (Pannoramic, 3D Hitech, Hungary).

2.4.5. Characterization of the stented arteries

Stented coronary arteries were explanted, washed with heparin solution (100 units/mL) and fixed in 10% paraformaldehyde for 24 h before final processing. The tissue was then dehydrated and infiltrated with resin (Light polymerizing Kulzer, EXAKT, Germany). The tissue was embedded in resin and polymerized by light of different wavelengths (white/blue light) for 10 h. A thin section as thin as 100 μ m was cut and further ground to 15 μ m by a micro grinding system (E400CS, EXAKT, Germany) for subsequent staining. The cross-sectional slices were stained with hematoxylin and then used for histomorphometric analysis.

The stented coronary arteries for endothelialization analysis were cut longitudinally and fixed in 2.5% glutaraldehyde for 24 h before final processing. Scanning electron microscopy was performed at 1 month post-stenting for the analysis of endothelialization according to previously published methods [18].

2.5. Statistical analysis

All quantitative data are presented as the mean \pm SD (standard deviation). Statistical differences between groups were analyzed by one-way ANOVA and Tukey's multiple comparison test with Prism[®] 9. P values < 0.05 were considered to be statistically significant between groups.

3. Results and discussion

3.1. Characterization

This study used a coaxial electrospinning process to incorporate TEMPOL and RAPA into nanofibers (Fig. 1a–d). For preparation of uniform nanofibers, polymers with good electrospinnability (PLA and PVA) were selected for electrospinning [19]. Given the poor water solubility of RAPA and the good water solubility of TEMPOL, RAPA was dissolved in the PLA/HFIP solution and loaded in the shell layer, while TEMPOL dissolved in the PVA aqueous solution and loaded in the core (Fig. 1a). To release TEMPOL and RAPA topically to the broken vascular intima, we collected the nanofibers and coated them onto the bare metal stents. As shown in Fig. 1b, the struts and gap of the stent were coated with the as-obtained nanofibers, indicating that a good coating of RAPA/TEMPOL nanofibers covered the stent plating area. For the micromorphology of such nanofibers, the as-electrospun nanofibers in such a coaxial electrospinning system presented a core-shell structure with a clear boundary (Fig. 1c). The surface morphology of the as-electrospun membranes with different loading amounts of TEMPOL and RAPA was demonstrated by SEM (Fig. 1d and Fig. S1). As shown in these SEM images, all fibers were smooth and randomly oriented with no visible beads-on-a-string or spindles-on-a-string phenomena and had close mean diameters. SEM images of P-R1-T2 and P-R0-T0 showed that the fiber diameter distribution is more concentrated for P-R1-T2 than for P-R0-T0 (Fig. 1d). This result indicated that the addition of TEMPOL and RAPA improved the uniformity of the nanofibers.

3.2. *In vitro* release of TEMPOL and RAPA

Compared with the coating of commercial DES (spray or dip coating), nanofiber membrane coating provides the stent with sustained

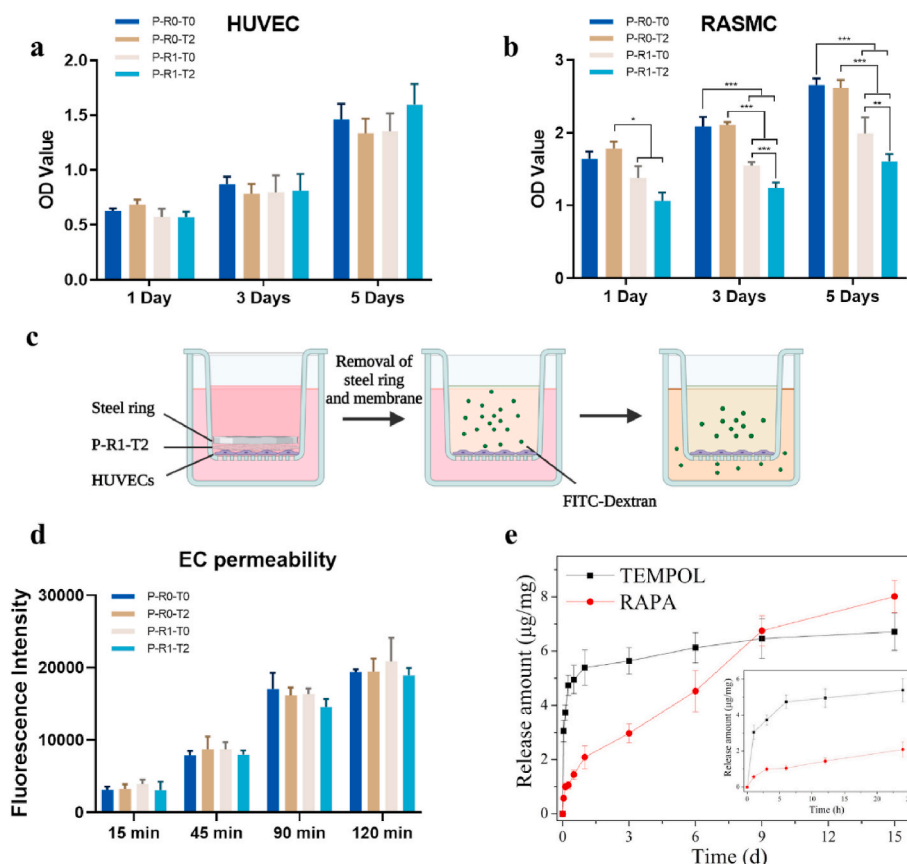


Fig. 2. Cytocompatibility and *in vitro* release behavior of RAPA/TEMPOL-loaded nanofiber membranes. The viability of (a) HUVECs or (b) RASMCs on nanofiber membranes for 1 day, 3 days and 5 days (mean \pm SD, $n = 5$ independent samples); Schematic illustration (c) and quantitative analysis (d) of the permeability of HUVECs cultured with nanofiber membranes using a FITC-dextran infiltration model (mean \pm SD, $n = 3$ independent samples). (e) TEMPOL and RAPA *in vitro* release curves of the P-R1-T2 nanofiber membrane (mean \pm SD, $n = 3$ independent samples). One-way ANOVA and Tukey's multiple comparison test were performed to determine the differences among various membranes. Statistically significant differences are indicated by * $P < 0.05$, ** $P < 0.01$, or *** $P < 0.001$.

drug release profile, and synergical release of one more drug with the structure design of nanofiber. *In vitro* release measurements were conducted on the RAPA/TEMPOL-loaded PLA electrospun membranes using HPLC to monitor their release behaviors. As shown in Fig. 2e, it was found that the release behavior of both TEMPOL and RAPA experienced two stages: the initial burst release on the first day and the continuous slow release on the following days. The initial burst release is mainly attributed to the diffusion of TEMPOL and RAPA on the surface of the nanofibers [20]. In the stage of continuous slow release, the release rates of TEMPOL and RAPA slowed down; the release amount of TEMPOL gradually tended to be stable after the first day, while that of RAPA maintained a significant increase. This finding is because RAPA is more hydrophobic than TEMPOL and is not easy to dissolve in a water solution, so it exhibits more lasting *in vitro* release. Based on the *in vitro* release property of P-R1-T2, we selected the third day (TEMPOL was mostly released) as the time point to study how P-R1-T2 affected the *in vitro* behaviors of HUVECs and RASMCs with TEMPOL and RAPA.

3.3. *In vitro* cytocompatibility

The antiproliferative agents in the DES coating are effective in inhibiting VSMC proliferation. However, the antiproliferative stent coating can also delay re-endothelialization in the stented segment, contributing to late in-stent thrombosis events. The concern of in-stent thrombosis has led to the extended duration of dual antiplatelet therapy [21–23]. Thus, an ideal stent coating must inhibit vicinal VSMCs while promoting the regeneration ability and preserving the functions of ECs [24–26].

Previous studies have reported that TEMPOL can inhibit VSMC migration, while such an effect does not act on ECs [11]. To further complement this effect, we incorporated RAPA into this system. We started our investigation by evaluating EC and VSMC proliferation on

RAPA/TEMPOL-loaded membranes. CCK-8 assays were performed 1 day, 3 days and 5 days after seeding ECs and VSMCs on the membranes. None of the membranes caused a significant inhibition of cell viability of ECs at 1 day and 3 days (Figs. 2a and S2a). Nevertheless, membranes incorporated with a high concentration of TEMPOL (P-R1-T10) exhibited a significant inhibitory effect toward ECs with or without rapamycin at 5 days (Figs. 2a and S2a), which was also shown in our previous study [11]. The viability of adherent VSMCs was not changed by TEMPOL incorporation at any time point. Alternatively, significant inhibition of VSMC viability was observed in the RAPA group. Notably, TEMPOL enhanced the VSMC inhibition ability of the RAPA-loaded membranes. The P-R1-T2 group exhibited higher VSMC inhibition than either the P-R1-T0 or P-R0-T2 group (Figs. 2b and S2b). A further increase in TEMPOL loading (P-R1-T10) did not enhance the antiproliferative ability of the membrane. In contrast, P-R1-T2 exhibited a significantly stronger antiproliferative effect on VSMCs than P-R1-T10. The above results indicate that the P-R1-T2 membrane has the best inhibition of VSMCs while sparing ECs.

In addition to EC proliferation and viability, endothelial permeability is crucial in determining endothelial barrier formation [27]. RAPA was reported to impair endothelial barrier function by downstream disruption of p120-VE cadherin in vascular endothelium [28]. Thus, we measured TEMPOL- and RAPA-induced alterations in endothelial barrier function by an *in vitro* dextran diffusion permeability assay (a schematic illustration is shown in Fig. 2c). The P-R1-T2 group did not show more dextran diffusion to the lower chamber than the control membrane group at any time point (Fig. 2d). To the best of our knowledge, the results suggest that concentrations of RAPA did not reach the threshold of endothelial barrier disruption.

To further study the cellular inhibitory effect of RAPA/TEMPOL-loaded nanofibers, we conducted a live/dead assay to evaluate the cell death status of VSMCs grown on the membranes. As shown in Fig. 3a and Fig. S3, P-R0-T0 and TEMPOL incorporation did not change the cell death status of VSMCs. However, RAPA caused nearly 50% VSMC death (Fig. 3c). The combination of RAPA and TEMPOL did not further increase VSMC death observed on the membranes.

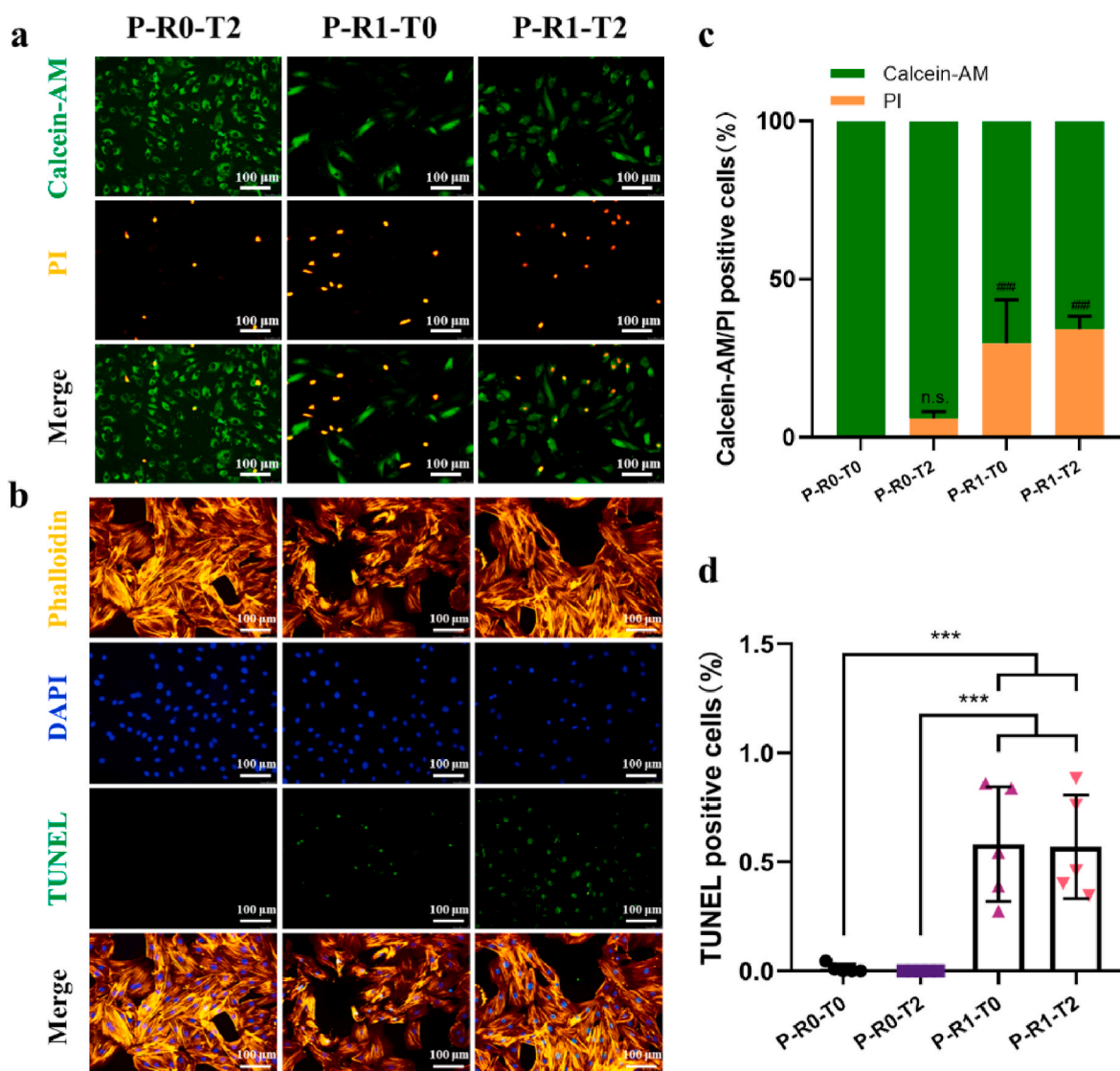


Fig. 3. Effect of the RAPA/TEMPOL-loaded nanofiber membrane on the cellular status of VSMCs. RASMCs were incubated for 3 days on nanofiber membranes. (a) Calcein-AM/PI staining fluorescence images displaying live (green) and dead (gold) RASMCs seeded onto various membranes (mean \pm SD, $n = 3$ independent samples). (b) TUNEL and phalloidin costaining fluorescence images displaying apoptotic RASMCs (green) seeded onto various membranes (mean \pm SD, $n = 5$ independent samples). (c, d) Quantitative analysis of live/dead and apoptotic cells. One-way ANOVA and Tukey's multiple comparison test were performed to determine the differences among various membranes. Statistically significant differences are indicated by *n.s.* not significant, *** $P < 0.001$; ### $P < 0.001$ compared with P-R0-T0.

Moreover, fluorescence staining was then performed to evaluate the apoptosis of VSMCs cultured on membranes using TUNEL assays (Figs. 3b and S4). The results showed that the number of apoptotic cells was rarely observed in the control and TEMPOL groups. However, after 3 days of culture, the apoptotic rates in the P-R1-T0 and P-R1-T2 groups were 58.1% and 57.0%, respectively (Fig. 3d). On the P-R1-T0 and P-R1-T2 membranes, the number of apoptotic cells was significantly higher but did not show a difference between the two groups, which is consistent with the live/dead assay results. Notably, VSMC morphology was shifted from a spindle shape to an irregular “dying” shape after RAPA incorporation. This result indicates that RAPA can directly induce VSMC apoptosis. TEMPOL can act with rapamycin to inhibit VSMC proliferation yet shows no effect on cell death or apoptosis of VSMCs. Above all, we preliminarily believe that a proper amount of TEMPOL can act with RAPA in VSMC inhibition while preserving endothelial barrier function.

3.4. ROS scavenging and anti-inflammatory effects on endothelial cells

In addition to delayed endothelial healing associated with anti-proliferative drugs eluting from DESs, stent-induced or polymer-induced

inflammation has also been identified as an essential factor in stent thrombosis [29–31]. Inflammatory responses to drugs, stents, or polymers may result from nonspecific innate immune responses and ROS production [32]. Several studies have also identified stent-induced ROS production and inflammation in the pathobiology of restenosis, stent thrombosis and vasomotor disturbance [33–35].

Oxidative stress refers to the production of reactive oxygen species (ROS) and the resulting intracellular antioxidant imbalance, leading to a series of cellular dysfunctions. To study the ROS scavenging activity of RAPA/TEMPOL-loaded nanofiber membranes in vascular cells, we used DCFH-DA as a probe to fluorescently monitor the total intracellular ROS levels. Flow cytometry allowed the quantitative evaluation of cellular ROS levels. The results of flow cytometry of ROS are shown in Fig. S5. As expected, the ROS level markedly increased in the H₂O₂-treated groups at 16 h. However, the TEMPOL-loaded nanofiber membranes could counterbalance the ROS level increase in the ECs stimulated by H₂O₂, while RAPA did not further improve the ROS scavenging effect.

The de novo synthesis of cell adhesion molecules (e.g., VCAM-1 and E-selectin) of endothelial cells is known to occur in cases of vascular injury and inflammation [36]. We thus examined whether the expression of VCAM-1 and E-selectin can be inhibited by the membrane in an *in*

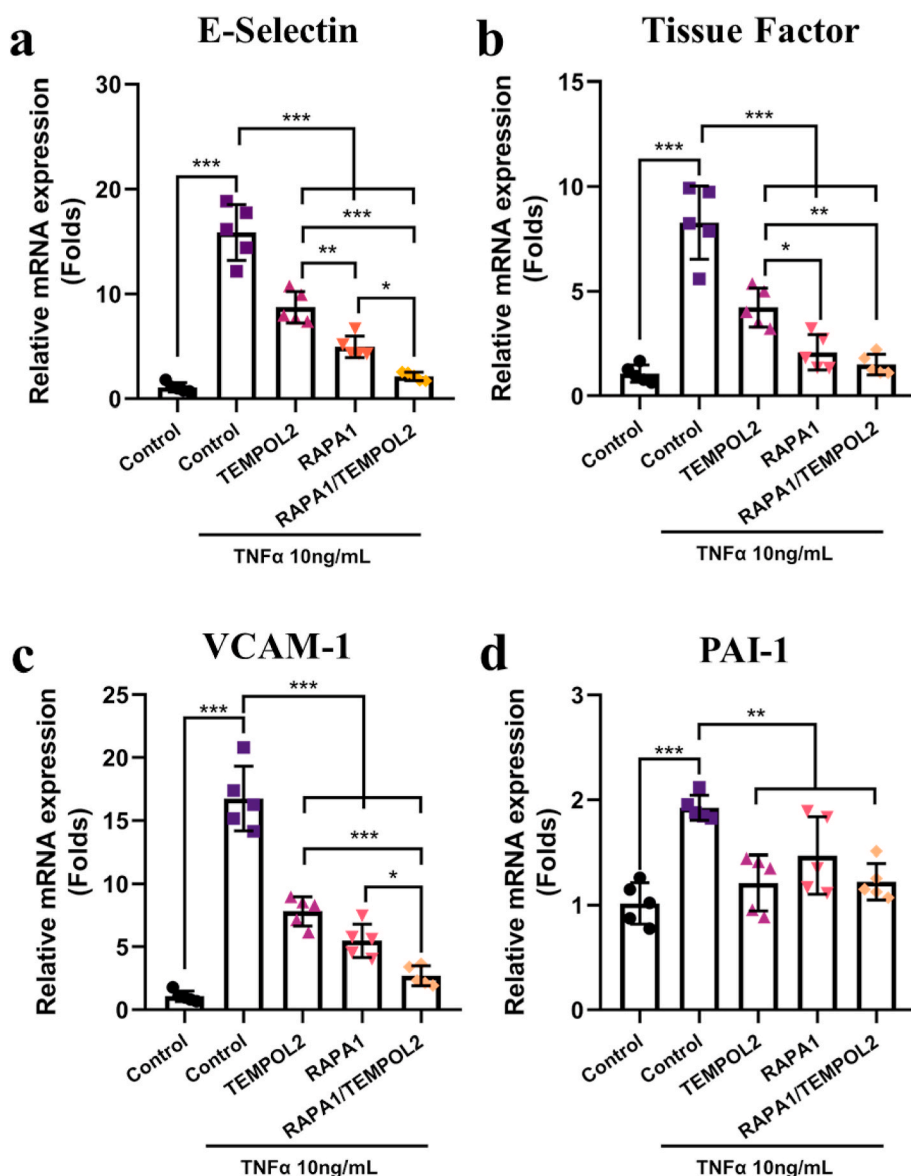


Fig. 4. Inhibition of adhesive molecules and pro-thrombotic factor expression in HUVECs. HUVECs were incubated with nanofiber membranes for 3 days before stimulation with 10 ng/mL TNF α for 2 h; qRT-PCR analysis of E-selectin (a), VCAM-1 (b), TF (c) and PAI-1 (d) mRNA expression showing the anti-inflammatory and antithrombotic performance of membranes in HUVECs (mean \pm SD, n = 5 independent samples). One-way ANOVA and Tukey’s multiple comparison test were performed to determine the differences among various membranes. Statistically significant differences are indicated by * P < 0.05, ** P < 0.01, or *** P < 0.001.

in vitro endothelial injury model. The mRNA expression of VCAM-1 (Fig. 4a) and E-selectin (Fig. 4b) was markedly elevated after TNF α treatment at 2 h. Compared with the control cells, the HUVECs cultured on the TEMPOL- and RAPA-loaded nanofiber membranes presented significantly reduced mRNA expression of VCAM-1 and E-selectin. Notably, the nanofibers with both TEMPOL and RAPA further reduced VCAM-1 and E-selectin levels. Stent implantation was reported to stimulate the release of TNF α from activated inflammasomes in target lesions, which could induce persistent vascular inflammation by activating signaling pathways in ECs [37]. TEMPOL was able to stop this process by ROS scavenging, which led to impediment of inflammasome activation. Therefore, the results indicated better inhibition of inflammation in the P-R1-T2 group, which is in line with the clinical expectations of stents in terms of inhibiting inflammation.

Vascular endothelial cells produce many modulatory proteins, such as tissue factor (TF) and plasminogen activator inhibitor-1 (PAI-1), which accelerate the development of thrombotic states in response to inflammation or injury [38]. Thus, the inhibitory effect of membranes on prothrombotic factors was evaluated. RAPA/TEMPOL-loaded nanofiber membranes rescued the TF (Fig. 4c) and PAI-1 (Fig. 4d) elevation in the HUVECs stimulated by TNF α . These data demonstrate that only the P-R1-T2 membrane achieved the optimal combination of all these effects when compared to the RAPA and TEMPOL only membranes. Consistent with our previous work demonstrating that TEMPOL drives ROS balance, guaranteeing vascular homeostasis, we believe that RAPA and TEMPOL, with the nanofiber membrane delivery system, act together to reduce the risk of inflammation and in-stent thrombosis.

3.5. *In vitro* effects on the biological function of vascular smooth muscle cells

In response to vascular injury, activated inflammatory cells, platelets and VSMCs release growth factors, especially PDGF, thereby leading to a switch of VSMCs from a quiescent, contractile phenotype to a dedifferentiated, synthetic phenotype [39]. This phenotypic switching process is characterized by downregulation of the expression of VSMC contractile markers such as CNN1 and SM22 α as well as upregulation of synthetic protein expression of OPN. In addition, ROS were reported to participate in VSMC phenotypic switching by activating the NF κ B signaling cascade in response to vascular injury [40]. Our previous work also showed that TEMPOL could attenuate PDGF-BB-triggered VSMC migration by ROS scavenging. Moreover, mTOR is responsible for VSMC dedifferentiation and proliferation; thus, inhibition of mTOR by RAPA can effectively maintain the contractile phenotype of VSMCs [40]. Thus, we next examined whether RAPA and TEMPOL have synergistic effects on PDGF-BB-induced ROS production and VSMC phenotypic switching.

Consistent with findings in ECs, TEMPOL-loaded nanofiber membranes reduced VSMC ROS levels stimulated by PDGF-BB, while RAPA incorporation further lowered the ROS levels (Figs. S5b and S5d). We examined the proliferation of VSMCs subjected to PDGF-BB stimulation by performing EdU assays (a schematic illustration is shown in Fig. 5a). As shown in Fig. 5c, the percentage of EdU-positive cells significantly increased from $28.7 \pm 7.5\%$ to $63.0 \pm 12.2\%$ after PDGF-BB stimulation. TEMPOL and RAPA significantly attenuated VSMC proliferation with PDGF-BB stimulation, and the EdU-positive cells were $44.7 \pm 4.6\%$ and $28.9 \pm 4.0\%$, respectively. The combination of RAPA and TEMPOL further inhibited VSMC proliferation below physiological levels ($12.1 \pm 2.9\%$).

Western blotting was further performed to determine the function of RAPA/TEMPOL-loaded nanofiber membranes on VSMC phenotypic switch biomarkers. As shown in Fig. 5d, the TEMPOL group and RAPA group showed an obviously reversed PDGF-BB-triggered VSMC phenotypic switch from contractile to synthetic cells by upregulating CNN1 (Fig. 5e) and SM22 α protein levels (Fig. 5h) as well as downregulating OPN protein expression (Fig. 5f). Combining TEMPOL with RAPA further promoted this process. Moreover, the abnormal changes in the

cellular proliferation marker PCNA (Fig. 5g) were significantly suppressed in the RAPA group and P-R1-T2 group. VSMCs play a central role in neointima formation, vascular remodeling, and progression to in-stent restenosis after stent deployment. VSMCs undergo profound modifications during these processes. They switch to a synthetic phenotype and acquire high proliferative and migratory capacities. Thus, the current attempt to influence the phenotypic switch process of VSMCs by ROS scavenging could be instrumental in designing stent coatings that prevent in-stent restenosis.

3.6. Effect of RAPA/TEMPOL-loaded covered stents on in-stent restenosis and strut endothelialization

Encouraged by the results above, we coated BMS with P-R1-T2 nanofibrous membranes and implanted them into porcine coronary arteries. The *in situ* endothelialization ability and inhibition of excessive intimal hyperplasia were evaluated. BMS of 316L stainless steel and rapamycin-eluting commercialized DES were used as controls. Three groups of stents were randomly implanted in the LAD, LCX and RCA of Bama mini pigs. All stents were implanted with the guidance of real-time OCT coregistration with angiography. Complete stent apposition was achieved immediately after stent implantation (Fig. S6). The implantation procedure and angiographical follow-up are shown in Fig. S7. Coronary angiography and OCT were repeated at the 2 weeks-1 month-3 months follow-up. OCT imaging at any time point showed no noticeable stent area differences in the three groups (Fig. 6d), indicating sufficient radial force for either group. However, the mean luminal area of the RTCS group ($5.57 \pm 0.21 \text{ mm}^2$) was significantly larger than that of the BMS group ($4.94 \pm 0.26 \text{ mm}^2$) at 12 weeks of follow-up (Fig. 6c). Luminal area stenosis (AS, expressed as % of the lumen area traced on native lumen contrast OCT images) was analyzed in each of the three stent groups from 5 pigs at 2 weeks-1 month-3 months of consecutive OCT follow-up after stent implantation ($n = 5$ stents/group). The neointima area of the BMS group was $0.72 \pm 0.20 \text{ mm}^2$ at 2 weeks and $1.03 \pm 0.11 \text{ mm}^2$ at 1 month and reached $1.70 \pm 0.27 \text{ mm}^2$ at 3 month post-implantation. AS increased from $10.93 \pm 2.89\%$ to $25.31 \pm 3.45\%$ during that time (Fig. 6e and f). Upon loading of the RAPA coating, DES strongly inhibited neointimal hyperplasia. The neointima area and AS for DES were $0.53 \pm 0.12 \text{ mm}^2$ and $8.14 \pm 2.03\%$, respectively, at 1 month. Nevertheless, the neointimal inhibitory effect seems unsustainable, as we found that the indices increased to $0.93 \pm 0.24 \text{ mm}^2$ and $14.27 \pm 3.94\%$ at 3 month. In comparison, RTCS demonstrated slow and steady neointima growth since the neointima area was slightly enhanced from $0.68 \pm 0.20 \text{ mm}^2$ at 1 month to $0.82 \pm 0.17 \text{ mm}^2$ at 3 month. The degree of stenosis and neointimal area in the BMS group were consistently greater than those in the RTCS group and DES group after 1 month (Fig. 6e and f). The result was confirmed by histomorphometric observation of hematoxylin-eosin-stained cross-sections (Fig. 7e and f). Cross-sections of BMS-stented arteries showed neointimal hyperplasia and the presence of inflammatory cells surrounding stent struts at 3 month. In contrast, the extent of neointima and inflammation were lower in the RTCS and DES groups (Fig. 7c). On the other hand, as shown in Table S2, qualitative OCT analysis demonstrated the greatest incidence of uncovered struts in DES, while RTCS and BMS showed more stent coverage at 2 weeks ($20.33 \pm 5.36\%$, $47.19 \pm 12.14\%$, and $50.05 \pm 14.63\%$, respectively, $p = 0.0025$). At 1 month follow-up, half of the struts of DES were still uncovered, significantly higher than RTCS group. OCT images at 3 months showed almost complete strut coverage in all three groups.

To explain the difference among stent groups, we examined the ROS level of stented arteries at 1 month. Fluorescent images of the DHE-stained sections, allowing detection of ROS in the red channel, were used to evaluate the *in vivo* ROS scavenging ability of the RAPA/TEMPOL-loaded covered stents. Of note, in contrast to those of the BMS and DES groups, the ROS level in the RTCS group was lower in the arterial media and neointima of stented arteries (Fig. 7a, d and S8).

SEM was further performed to demonstrate the potential of the RTCS

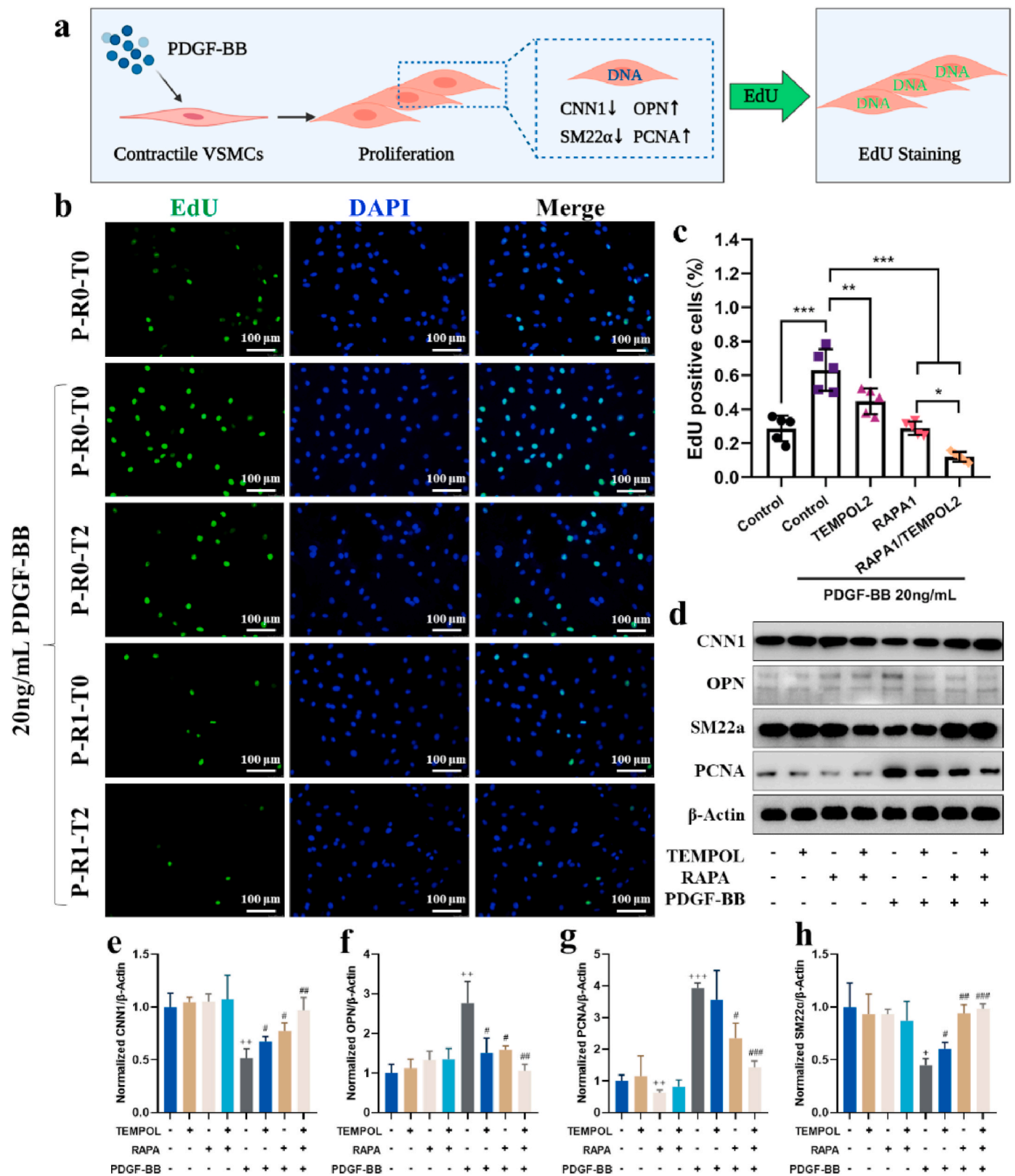


Fig. 5. Effects of the RAPA/TEMPOL-loaded nanofiber membrane on the PDGF-BB-induced phenotypic switch of VSMCs *in vitro*. RASMCs were seeded on nanofiber membranes and stimulated with PDGF-BB for 3 days. (a) Schematic illustration of VSMC phenotypic switching and EdU incorporation. (b) EdU assays indicating the antiproliferative properties of various membranes in RASMCs (mean ± SD, n = 5 independent samples). (d) Expression of the VSMC phenotypic biomarkers CNN-1, OPN, SM22a and PCNA detected by Western blots and (e–h) corresponding quantitative analysis (mean ± SD, n = 5 independent samples). One-way ANOVA and Tukey’s multiple comparison test were performed to determine the differences among various membranes. Statistically significant differences are indicated by **P* < 0.05, ***P* < 0.01, or ****P* < 0.001; +*P* < 0.05, ++*P* < 0.01, +++*P* < 0.001 compared with the P-R0-T0 group; #*P* < 0.05, ##*P* < 0.01, ###*P* < 0.001 compared with the P-R0-T0+PDGF-BB group.

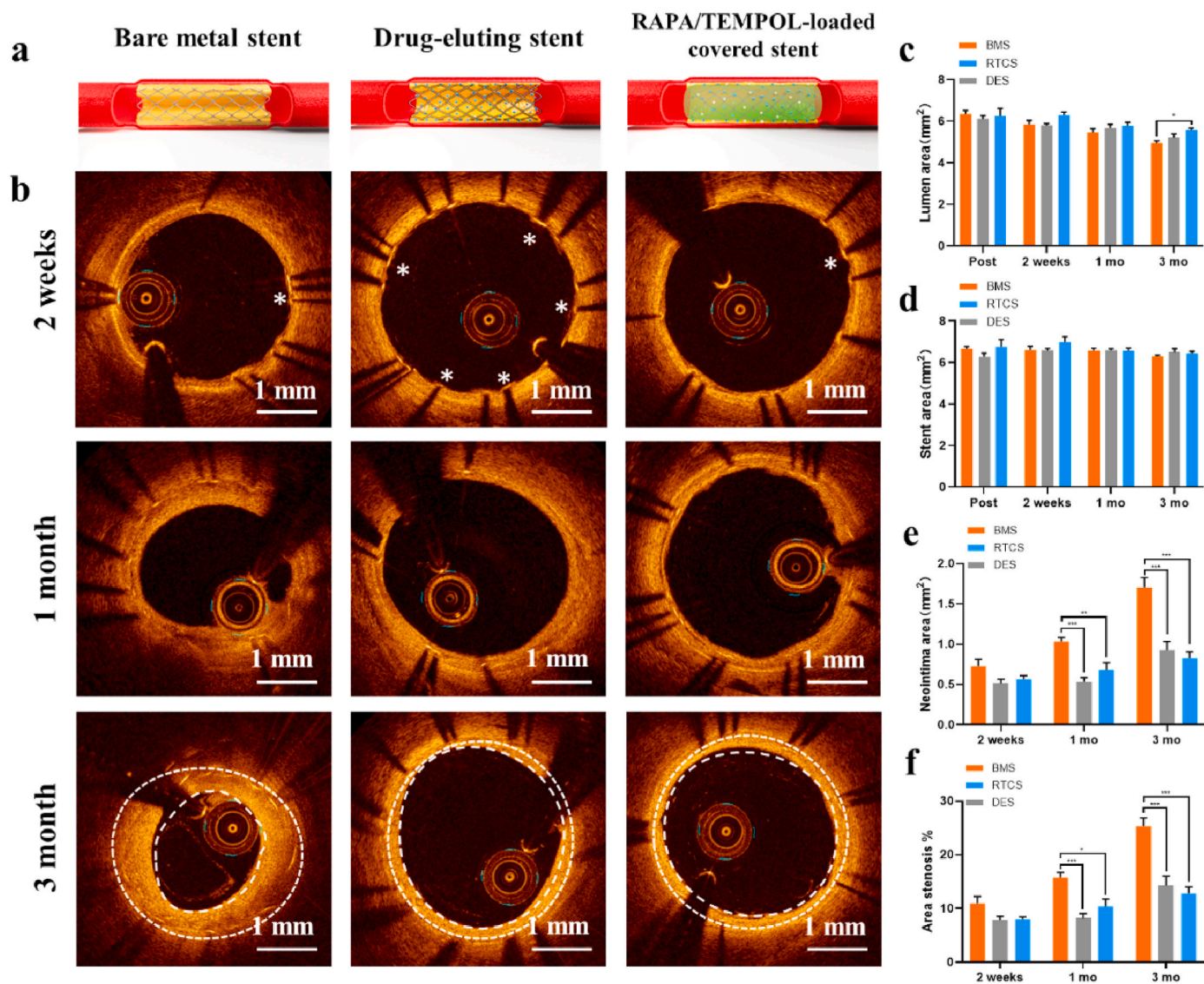


Fig. 6. *In vivo* evaluation of in-stent stenosis by optical coherence tomography. (a) Schematic illustration of neointimal hyperplasia of the BMS, DES and RTCS at the 3-month follow-up. (b) OCT was performed at 2 weeks, 1 month and 3 months post-implantation. Asterisks indicate uncovered stent struts. Broken lines indicate the stent contour (outside) and luminal contour (inside). Quantitative analysis of (c) the lumen area, (d) stent area, (e) neointima area and (f) area stenosis rate (mean \pm SD, $n = 5$ independent stented arteries). One-way ANOVA and Tukey's multiple comparison test were performed to determine the differences among various stents. Statistically significant differences are indicated by * $P < 0.05$, ** $P < 0.01$, or *** $P < 0.001$.

for re-endothelialization. SEM of the luminal side of stented arteries revealed that endothelialization was remarkably delayed on the DES compared with other stents at 1 month. Both the BMS and RTCS groups achieved a high grade of endothelialization, whose ECs were elongated and oriented in the direction of blood flow at 1 month (Fig. 7b).

Herein, we further report that RAPA/TEMPOL-loaded covered stents promote *in vivo* endothelial healing while reducing ROS production, leading to in-stent restenosis and inflammation compared to DES and BMS, respectively. While rapid endothelialization is achieved in the presence of BMS, ROS production and inflammation in vascular injury and the foreignness of metal struts eventually lead to in-stent restenosis [41]. The antistenotic effect of DES was counterbalanced by incomplete endothelialization at 1 month, consistent with previous studies [18]. Our study demonstrates that RTCS is efficient for both rapid endothelialization and ROS scavenging. This phenomenon leads to the formation of a seemingly healthy endothelial barrier with anti-inflammatory properties, and a thin neointimal layer resembles DES. We therefore believe that RAPA/TEMPOL-loaded nanofiber membranes are a feasible approach for stent coating and could meet the improvement expected in

the stent field. However, a long-term follow-up (≥ 6 months) and research in atheromatous animal models would be necessary for the translational perspective.

4. Conclusion

In this work, we developed a multifunctional drug-loaded nanofibrous stent coating through coaxial electrospinning with RAPA in the shell and TEMPOL in the core spinning solution. The RAPA/TEMPOL-loaded nanofiber membrane showed sustained and controlled drug release kinetics. Specifically, this membrane showed a great anti-proliferative and proapoptotic effect on arterial smooth muscle cells (RASMCs) while preserving endothelial barrier functions (HUVECs). Additionally, this membrane not only significantly mitigated TNF α -induced endothelial inflammation but also maintained the VSMC contractile phenotype under PDGF-BB stimulation through the synergistic effect of RAPA and the ROS scavenger TEMPOL. The *in vivo* results demonstrated that the RAPA/TEMPOL-loaded covered stents achieved ROS scavenging, rapid re-endothelialization, and effective prevention of

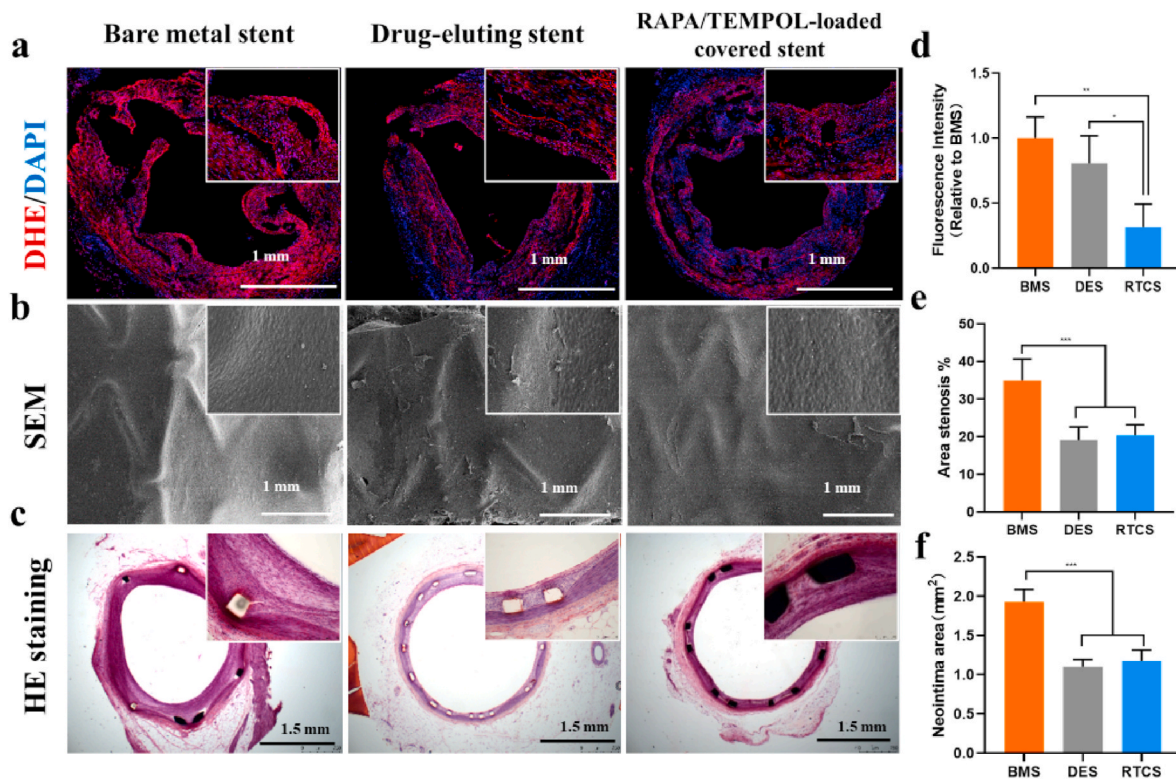


Fig. 7. *In vivo* evaluation of the re-endothelialization and ROS scavenging effects of RAPA/TEMPOL-loaded covered stents. (a) Fluorescence microscopy unveiling the ROS level of stented arteries. (blue: cell nucleus stained by DAPI, red: ROS stained by DHE). (b) SEM images showing the luminal faces of the stented arteries at 1 month post-stent deployment. (c) Representative images showing the cross-sections of the stented arteries after HE staining. (d) ROS fluorescence intensity relative to BMS group (mean \pm SD, $n = 3$ independent stented arteries). (e,f) Quantitative analyses of the area stenosis and neointima area in tissue sections (mean \pm SD, $n = 5$ independent stented arteries). One-way ANOVA and Tukey's multiple comparison test were performed to determine the difference among various stents. Statistically significant differences are indicated by *n.s.* not significant, $*P < 0.05$, $**P < 0.01$, or $***P < 0.001$.

in-stent restenosis. These RAPA/TEMPOL-loaded covered stents could combine neointima inhibition and rapid re-endothelialization, which provided a promising and effective method for addressing the major clinical complications of coronary stent implantation.

Ethical approval

All animal experiments were approved by the Ethics Committee of Zhongshan Hospital, Fudan University, Shanghai, China. The procedures were conducted conforming to the protocol established by the Experimental Animal Ethics branch.

CRediT authorship contribution statement

Rui Wang: Conceptualization, Investigation, Methodology, Writing – original draft. **Jian Lu:** Conceptualization, Formal analysis, Writing – original draft. **Jiasheng Yin:** Writing – original draft, Investigation, Resources. **Han Chen:** Investigation, Methodology. **Hongmei Liu:** Investigation. **Fei Xu:** Validation, Resources. **Tongtong Zang:** Methodology. **Rende Xu:** Methodology, Investigation. **Chenguang Li:** Resources. **Yizhe Wu:** Resources. **Qilin Wu:** Methodology. **Xiang Fei:** Writing – review & editing. **Meifang Zhu:** Supervision, Funding acquisition. **Li Shen:** Methodology, Writing – review & editing, Funding acquisition. **Junbo Ge:** Conceptualization, Supervision, Funding acquisition, Writing – review & editing.

Declaration of competing interest

The authors declare that they have no known competing financial interests or personal relationships that could have appeared to influence

the work reported in this paper.

Acknowledgments

This work was financially supported by the National Natural Science Foundation of China (No. 82170342), the Shanghai Engineering Research Center of Interventional Medicine (No. 19DZ2250300), the National Key R&D Program of China (No. 2021YFA1201300 and No. 2020YFC1316703), the Chinese Academy of Medical Sciences (2019-I2M-5-060 and 2020-JKCS-0154020) and the Shanghai Shenkang Hospital Development Center (SHDC2020CR3023B). We gratefully acknowledge Mr. H. Ren for the help with stent preparation and Mr. X. Yan for providing the bare metal stents. We thank Mr. C. Li from the Shanghai Institute of Cardiovascular Diseases for assistance with the flow cytometry.

Appendix A. Supplementary data

Supplementary data to this article can be found online at <https://doi.org/10.1016/j.bioactmat.2022.04.033>.

References

- [1] N. Townsend, L. Wilson, P. Bhatnagar, K. Wickramasinghe, M. Rayner, M. Nichols, Cardiovascular disease in Europe: epidemiological update 2016, *Eur. Heart J.* 37 (42) (2016) 3232–3245.
- [2] S. Liu, Y. Li, X. Zeng, H. Wang, P. Yin, L. Wang, et al., Burden of cardiovascular diseases in China, 1990–2016: findings from the 2016 global burden of disease study, *JAMA Cardiol.* 4 (4) (2019) 342–352.
- [3] X. Zheng, J.P. Curtis, S. Hu, Y. Wang, Y. Yang, F.A. Masoudi, et al., Coronary catheterization and percutaneous coronary intervention in China: 10-year results from the China PEACE-retrospective CathPCI study, *JAMA Intern. Med.* 176 (4) (2016) 512–521.

- [4] D.J. Holmes, D.P. Taggart, Revascularization in stable coronary artery disease: a combined perspective from an interventional cardiologist and a cardiac surgeon, *Eur. Heart J.* 37 (24) (2016) 1873–1882.
- [5] G.W. Stone, J.F. Sabik, P.W. Serruys, C.A. Simonton, P. Généreux, J. Puskas, et al., Everolimus-eluting stents or bypass surgery for left main coronary artery disease, *N. Engl. J. Med.* 375 (23) (2016) 2223–2235.
- [6] R.P. Juni, H.J. Duckers, P.M. Vanhoutte, R. Virmani, A.L. Moens, Oxidative stress and pathological changes after coronary artery interventions, *J. Am. Coll. Cardiol.* 61 (14) (2013) 1471–1481.
- [7] T. Inoue, K. Croce, T. Morooka, M. Sakuma, K. Node, D.I. Simon, Vascular inflammation and repair: implications for re-endothelialization, restenosis, and stent thrombosis, *JACC Cardiovasc. Interv.* 4 (10) (2011) 1057–1066.
- [8] M.C. Morice, P.W. Serruys, J.E. Sousa, J. Fajadet, H.E. Ban, M. Perin, et al., A randomized comparison of a sirolimus-eluting stent with a standard stent for coronary revascularization, *N. Engl. J. Med.* 346 (23) (2002) 1773–1780.
- [9] E. Solinas, G. Dangas, A.J. Kirtane, A.J. Lansky, T. Franklin-Bond, P. Boland, et al., Angiographic patterns of drug-eluting stent restenosis and one-year outcomes after treatment with repeated percutaneous coronary intervention, *Am. J. Cardiol.* 102 (3) (2008) 311–315.
- [10] A.V. Finn, G. Nakazawa, M. Joner, F.D. Kologdie, E.K. Mont, H.K. Gold, et al., Vascular responses to drug eluting stents: importance of delayed healing, *Arterioscler. Thromb. Vasc. Biol.* 27 (7) (2007) 1500–1510.
- [11] J. Lu, R. Wang, L. Shen, J. Yin, G. Liu, H. Chen, et al., Enabling topical and long-term anti-radical properties for percutaneous coronary intervention-related complications by incorporating TEMPOL into electrospun nanofibers, *Sci. China Mater.* 64 (3) (2021) 769–782.
- [12] D.K. Jagadeesha, F.J. Miller, R.C. Bhalla, Inhibition of apoptotic signaling and neointimal hyperplasia by tempol and nitric oxide synthase following vascular injury, *J. Vasc. Res.* 46 (2) (2009) 109–118.
- [13] W. Huang, M. Huo, N. Cheng, R. Wang, New forms of electrospun nanofibers applied in cardiovascular field, *Front. Cardiovasc. Med.* 8 (2021) 801077.
- [14] M. Rafique, T. Wei, Q. Sun, A.C. Midgley, Z. Huang, T. Wang, et al., The effect of hypoxia-mimicking responses on improving the regeneration of artificial vascular grafts, *Biomaterials* 271 (2021) 120746.
- [15] Z. Shi, Y. Zhou, T. Fan, et al., Inorganic nano-carriers based smart drug delivery systems for tumor therapy, *Smart Mater. Med.* 1 (2020) 32–47.
- [16] Y. Hou, X. Deng, C. Xie, Biomaterial surface modification for underwater adhesion, *Smart Mater. Med.* 1 (2020) 77–91.
- [17] P.W. Serruys, Y. Onuma, J.A. Ormiston, B. de Bruyne, E. Regar, D. Dudek, et al., Evaluation of the second generation of a bioresorbable everolimus drug-eluting vascular scaffold for treatment of de novo coronary artery stenosis: six-month clinical and imaging outcomes, *Circulation* 122 (22) (2010) 2301–2312.
- [18] A.P. de Prado, C. Pérez-Martínez, C. Cuellas-Ramón, J.M. Gonzalo-Orden, M. Regueiro-Purriños, B. Martínez, et al., Time course of reendothelialization of stents in a normal coronary swine model: characterization and quantification, *Vet. Pathol.* 48 (6) (2011) 1109–1117.
- [19] H. Bi, T. Feng, B. Li, Y. Han, In vitro and in vivo comparison study of electrospun PLA and PLA/PVA/SA fiber membranes for wound healing, *Polymers* 12 (4) (2020).
- [20] A. Yin, R. Luo, J. Li, X. Mo, Y. Wang, X. Zhang, Coaxial electrospinning multicomponent functional controlled-release vascular graft: optimization of graft properties, *Colloids Surf. B Biointerfaces* 152 (2017) 432–439.
- [21] E.P. McFadden, E. Stabile, E. Regar, E. Cheneau, A.T. Ong, T. Kinnaird, et al., Late thrombosis in drug-eluting coronary stents after discontinuation of antiplatelet therapy, *Lancet (N. Am. Ed.)* 364 (9444) (2004) 1519–1521.
- [22] T. Palmerini, G. Biondi-Zoccai, R.D. Della, A. Mariani, P. Genereux, A. Branzi, et al., Stent thrombosis with drug-eluting stents: is the paradigm shifting? *J. Am. Coll. Cardiol.* 62 (21) (2013) 1915–1921.
- [23] P. Garg, L. Mauri, The conundrum of late and very late stent thrombosis following drug-eluting stent implantation, *Curr. Opin. Cardiol.* 22 (6) (2007) 565–571.
- [24] Y. Chen, P. Gao, L. Huang, X. Tan, N. Zhou, T. Yang, et al., A tough nitric oxide-eluting hydrogel coating suppresses neointimal hyperplasia on vascular stent, *Nat. Commun.* 12 (1) (2021) 7079.
- [25] Z. Yang, X. Zhao, R. Hao, Q. Tu, X. Tian, Y. Xiao, et al., Bioclickable and mussel adhesive peptide mimics for engineering vascular stent surfaces, *Proc. Natl. Acad. Sci. U. S. A.* 117 (28) (2020) 16127–16137.
- [26] Y. Yang, P. Gao, J. Wang, Q. Tu, L. Bai, K. Xiong, et al., Endothelium-mimicking multifunctional coating modified cardiovascular stents via a stepwise metal-catechol-(amine) surface engineering strategy, *Research (Wash D C)* 2020 (2020) 9203906.
- [27] A. Sakamoto, S. Torii, H. Jinnouchi, L. Guo, A. Cornelissen, S. Kuntz, et al., Comparison of endothelial barrier functional recovery after implantation of a novel biodegradable-polymer sirolimus-eluting stent in comparison to durable- and biodegradable-polymer everolimus-eluting stents, *Cardiovasc. Revascularization Med.* 24 (2021) 1–10.
- [28] A. Habib, V. Karmali, R. Polavarapu, H. Akahori, Q. Cheng, K. Pachura, et al., Sirolimus-FKBP12.6 impairs endothelial barrier function through protein kinase C- α activation and disruption of the p120-vascular endothelial cadherin interaction, *Arterioscler. Thromb. Vasc. Biol.* 33 (10) (2013) 2425–2431.
- [29] J.R. Nebeker, R. Virmani, C.L. Bennett, J.M. Hoffman, M.H. Samore, J. Alvarez, et al., Hypersensitivity cases associated with drug-eluting coronary stents: a review of available cases from the Research on Adverse Drug Events and Reports (RADAR) project, *J. Am. Coll. Cardiol.* 47 (1) (2006) 175–181.
- [30] R. Virmani, G. Guagliumi, A. Farb, G. Musumeci, N. Grieco, T. Motta, et al., Localized hypersensitivity and late coronary thrombosis secondary to a sirolimus-eluting stent: should we be cautious? *Circulation* 109 (6) (2004) 701–705.
- [31] M.A. Pallero, R.M. Talbert, Y.F. Chen, P.G. Anderson, J. Lemons, B.C. Brott, et al., Stainless steel ions stimulate increased thrombospondin-1-dependent TGF- β activation by vascular smooth muscle cells: implications for in-stent restenosis, *J. Vasc. Res.* 47 (4) (2010) 309–322.
- [32] R.A. Byrne, M. Joner, A. Kastrati, Polymer coatings and delayed arterial healing following drug-eluting stent implantation, *Minerva Cardioangiol.* 57 (5) (2009) 567–584.
- [33] G.E. Kochiadakis, D.A. Arfanakis, M.E. Marketou, E.I. Skalidis, N.E. Igoimenidis, D. Nikitovic, et al., Oxidative stress changes after stent implantation: a randomized comparative study of sirolimus-eluting and bare metal stents, *Int. J. Cardiol.* 142 (1) (2010) 33–37.
- [34] A. Jabs, S. Göbel, P. Wenzel, A.L. Kleschyov, M. Hortmann, M. Oelze, et al., Sirolimus-induced vascular dysfunction. Increased mitochondrial and nicotinamide adenine dinucleotide phosphate oxidase-dependent superoxide production and decreased vascular nitric oxide formation, *J. Am. Coll. Cardiol.* 51 (22) (2008) 2130–2138.
- [35] L.K. Pendyala, J. Li, T. Shinke, S. Geva, X. Yin, J.P. Chen, et al., Endothelium-dependent vasomotor dysfunction in pig coronary arteries with Paclitaxel-eluting stents is associated with inflammation and oxidative stress, *JACC Cardiovasc. Interv.* 2 (3) (2009) 253–262.
- [36] P.K. Shah, Inflammation, neointimal hyperplasia, and restenosis: as the leukocytes roll, the arteries thicken, *Circulation* 107 (17) (2003) 2175–2177.
- [37] J. Ma, X. Liu, L. Qiao, L. Meng, X. Xu, F. Xue, et al., Association between stent implantation and progression of nontarget lesions in a rabbit model of atherosclerosis, *Circ. Cardiovasc. Interv.* 14 (11) (2021), e10764.
- [38] S. Diaz-Rodriguez, C. Rasser, J. Mesnier, P. Chevallier, R. Gallet, C. Choqueux, et al., Coronary stent CD31-mimetic coating favours endothelialization and reduces local inflammation and neointimal development in vivo, *Eur. Heart J.* 42 (18) (2021) 1760–1769.
- [39] D. Gomez, G.K. Owens, Smooth muscle cell phenotypic switching in atherosclerosis, *Cardiovasc. Res.* 95 (2) (2012) 156–164.
- [40] Q.B. Lu, M.Y. Wan, P.Y. Wang, C.X. Zhang, D.Y. Xu, X. Liao, et al., Chicoric acid prevents PDGF-BB-induced VSMC dedifferentiation, proliferation and migration by suppressing ROS/NF κ B/mTOR/P70S6K signaling cascade, *Redox Biol.* 14 (2018) 656–668.
- [41] K. Ohtani, K. Egashira, Y. Ihara, K. Nakano, K. Funakoshi, G. Zhao, et al., Angiotensin II type 1 receptor blockade attenuates in-stent restenosis by inhibiting inflammation and progenitor cells, *Hypertension* 48 (4) (2006) 664–670.